Olefin Autoxidation in Flow

Citation: Neuenschwander, Ulrich, and Klavs F. Jensen. "Olefin Autoxidation in Flow." Ind. Eng. Chem. Res. 53, no. 2 (January 15, 2014): 601–608.

As Published: http://dx.doi.org/10.1021/ie402736j

Publisher: American Chemical Society (ACS)

Persistent URL: http://hdl.handle.net/1721.1/93162

Version: Author's final manuscript: final author's manuscript post peer review, without publisher's formatting or copy editing

Olefin Autoxidation in Flow

*Ulrich Neuenschwander, Klavs F. Jensen**

Department of Chemical Engineering, Massachusetts Institute of Technology,

77 Massachusetts Avenue, Cambridge MA 02139, USA.

*kfjensen@mit.edu

ABSTRACT: Handling hazardous multiphase reactions in flow brings not only safety advantages but also significantly improved performance, due to better mass transfer characteristics. In this report, we present a continuous microreactor setup, capable of performing olefin autoxidations with O_2, under solvent-free and catalyst-free conditions. Owing to the transparent reactor design, consumption of O_2 can be visually followed and exhaustion of the gas bubbles marks a clear end point along the channel length coordinate. Tracking the position of this end point enables measuring effective rate constants. The developed system was calibrated using the well-studied β-pinene substrate, and was subsequently applied to the synthetically interesting transformation of (+)-valencene to (+)-nootkatone. For the latter, a space-time yield was obtained that is at least three orders of magnitude larger than that realized with established biotechnology approaches.

KEYWORDS: microreactor – gas liquid reactions – kinetics – oxidation – nootkatone

INTRODUCTION

Synthesis in flow reactors has proven to be an enabling technology for safety-critical reactions.[1-4] Unlike in batch reactors, the thermal mass of reacting fluid is low at any time. The product stream can be thermally/chemically quenched continuously and safely stored in vessels,[5] immediately transferred into downstream processing units,[6,7] or even telescoped into subsequent reaction steps.[8-10] One category of reactions ideally suited for taking benefit of the advantages of flow chemistry are oxidations with O_2, so-called autoxidations, preferably for selective late-stage functionalization of fine chemicals.[11] Firstly, these reactions require good gas-to-liquid mass transfer and elevated gas pressures. Secondly, tight control over the critical reaction parameters (temperature, stoichiometry, conversion) is crucial, in order to ensure constant product quality and safe handling of the transiently appearing organic peroxides. Thirdly, the reactor material should be highly resistant against corrosion, due to the harsh, oxidative conditions. Fourthly, reacting organic material and oxygen under those conditions poses an inherent safety risk. Thus, the smaller the volumes of reacting fluid and the head-space are, the safer the process will be. The spiral Si/Pyrex microreactors developed in our group[12,13] meet all these requirements. The oxygen dosage (stoichiometry) can be accurately controlled, due to the elimination of head-space. Moreover, the passivated silicon oxide surface ensures chemical compatibility with the corrosive, oxidative conditions. These microreactors do not only provide large surface areas (10^4 m^2/m^3), which allows intimate gas-liquid contact (interfacial areas of about 5×10^3 m^2/m^3), but they are also moderately pressure and temperature tolerant (>30 atm, >300°C).[14] The combination of large interfacial area and elevated pressure is very promising in terms of gas-to-liquid mass transfer. If the ratio of volumetric gas and liquid flow rates does not deviate too much from unity, the flow pattern within the reactor channel is a regular Taylor flow, with

alternating gas bubbles and liquid slugs. The mass-transfer under such Taylor flow conditions is enhanced by internal recirculation within the liquid slugs.[15]

β-pinene (**1**, Scheme 1) is a relatively abundant, renewable raw material as a by-product in the kraft paper pulp process.[16] Oxidative functionalization of this olefin is not only facile, it can also be done regioselectively and under retention of the absolute configuration. The autoxidation of **1** has recently been studied by some of us under batch conditions.[17] The primary oxidation products consist of hydroperoxides (**2**, **3**), alcohols (**4**, **5**), carbonyls (**6**, **7**) and epoxide (**8**). After corresponding reduction of the peroxides with e.g. sodium thiosulfate,[18] these allylic oxidation products are an important feedstock for fragrance mixtures, due to their interesting organoleptic properties.[19] This oxidation can be carried out without the need of a catalyst, nor a solvent. In fact, when using solvents, chances are high that the latter undergo stoichiometric cooxidation under reaction conditions.[20]

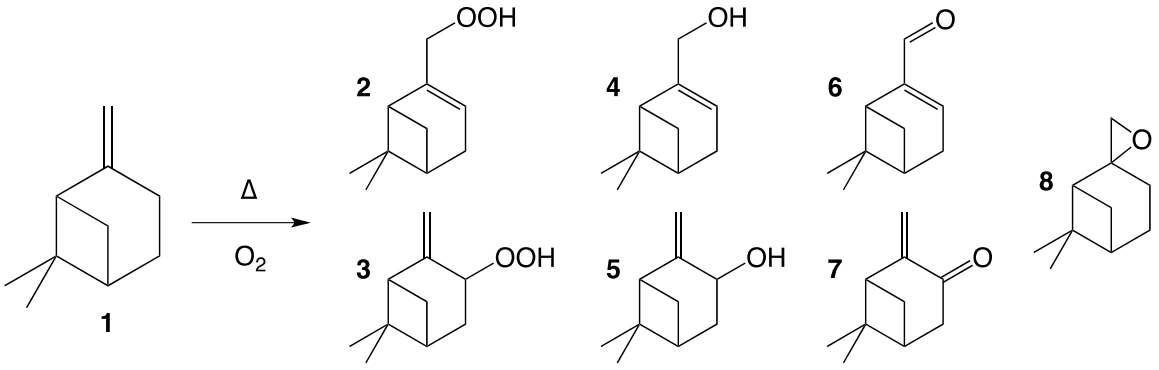

Scheme 1. Autoxidation of β-pinene (**1**).

In the case of olefins, the reaction mechanism is based on chain-propagating ROO• (i.e. peroxyl) radicals as in many other autoxidations. The product-catalyzed chain initiation[21] makes

the reaction autocatalytic, hence the term "autoxidation".[22] Under the bubble-column batch conditions in our earlier study, the reaction became mass-transfer limited at T ≥ 110°C.

(+)-valencene (**9**) is a naturally occuring sesquiterpene (i.e. $C_{15}H_{24}$, see Scheme 2). Along with limonene and myrcene, it is responsible for the fresh scent of oranges and therefore used as orange aroma in consumer products.[23] Traditionally, it has been extracted from harvested orange peel, which lead to some problems in supply fluctuation and pesticide co-extraction.[24] Its biosynthesis in Valencia oranges (*Citrus sinensis*) has been shown to occur via farnesyl pyrophosphate rearrangement in an enzyme called *Citrus Valencene Synthase* (CVS).[25] By incorporating the underlying gene into yeast cells, the two biotech companies *Allylix* and *Isobionics* have succeeded in developing a fermentation process that yields selectively **9**.[26] The market launch of biotechnological **9** was in 2010 for both companies.[27] As a consequence, the supply of **9** is more stable than it used to be.

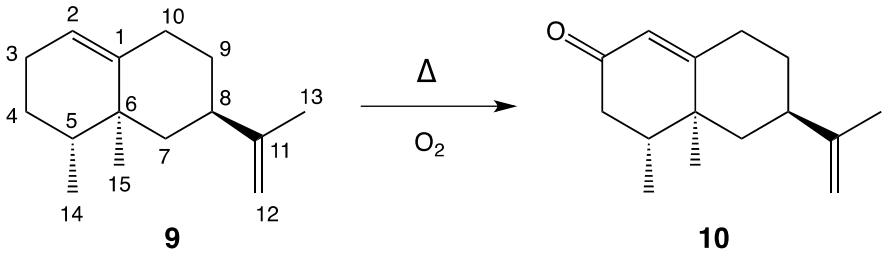

Scheme 2. Transformation of (+)-valencene (**9**) to (+)-nootkatone (**10**). The carbon centers susceptible to autoxidation are 1, 2, 3, 8, 10, 11, 12, 13.

The allylic oxidation of **9** to (+)-nootkatone (**10)** is a valuable transformation, since **10** is the main component of natural grapefruit flavour (Scheme 2).[28] It is used in the flavor and fragrance industry in a variety of grapefruit-tasting products (e.g. in beverages).[29] Again, the traditional extraction method requires enormous amounts of grapefruit peel[30] and is therefore not only

expensive but also subject to strong market supply fluctuations, caused by droughts or other harvesting shortages. The challenges with the synthesis of **10** are nicely reviewed by Zorn.[31] In general, biotechnological approaches towards **10** are abundant in the literature, working with plant cells,[32,33] animal cells,[34] bacteria,[35] fungi[36] or cell lyophilisates.[37,38] Those methods have proven to work quite selectively, albeit with very low space-time yields. In the conclusion of the above-mentioned review, Zorn declares that in spite of 40 years research, an industrially feasible synthesis process still remains to be established, in order to replace the traditional citrus pulp/peel extraction. The chemical synthesis approaches for this transformation do work in high yield, but rely on stoichiometric amounts of hazardous substances such as chromates[39] or metal/peroxide auxiliaries,[40-42] complicating uses of the processes for generation of **10** for food-applications

Even though autoxidation of **9** (i.e. direct oxidation with O_2) is a very promising approach and has been mentioned as a possibility to synthesize **10**,[31] it has not been explored extensively, possibly because of the tedious conditions in the original publication, such as the use of a solvent and initiator, and a low conversion after 90 h reaction time.[43] In this contribution, we show that **10** can be obtained by autoxidation of **9** in a microfluidic system, in competitive space-time yield, without the need for any additives, solvents, or initiators.

MATERIALS AND METHODS

Setup

The autoxidation experiments were carried out in a microfluidic setup (Figure 1, left) that allowed safe handling of this potentially hazardous chemistry. A heavy-duty syringe pump (PhD 2000, Harvard Apparatus), equipped with two pressure-resistant stainless steel syringes (Harvard Apparatus, 8 mL, teflon-greased), fed both gaseous (i.e. O_2) and liquid (i.e. neat organic liquids) reactants into the microreactor. Any contact of the oily substrate with the steel wall of the syringe could lead to leaching of ppm amounts of redox-active iron or to carry-over of some teflon grease into the thin reactor channels. Thus, instead of pumping the substrate directly, the syringe pumped water that pressed the oily substrate out of a prefilled 1/16" PFA tubing reservoir. We used a silicon-based microreactor with a spiral pattern (400 μm × 400 μm × 0.85 m = 136 μL), surface-passivated with SiO_2 and sealed with a transparent Pyrex lid.[12,13] In the development phase, silicon nitride coated microreactors were also tested. However, they were not suitable due to quick surface corrosion and partial plugging of the reactor channels. Note that the use of highly corrosion resistant metal alloys would also not be suitable for carrying out this type of chemistry, as those surfaces would be interfering with radical chemistry in increasing the rate of termination and thus artificially slowing down the overall kinetics. Cooling of the aluminum holder (chuck) connecting the microreactor to tubes from the pump was done with a recirculating chiller (ThermoFisher, Neslab RTE7). The reactor was heated by cartridge heaters imbedded in an aluminum frame that sandwiched the chip and a 5 mm Pyrex layer for mechanical stability. The latter layer also provided visual access to the reactor. Temperature was controlled with an appropriately tuned temperature controller (Omega, CN9412). The product mixture was collected in a 20 mL glass vial inside a 100 mL pressure

bomb that served as back-pressure regulator for the system. In order to keep the pressure bomb outside the explosion regime, it was prefilled with nitrogen prior to reaction. The bomb could have been continuously purged with nitrogen for the purpose of keeping the back-pressure exactly constant, but this was not done to prevent discontinuities in the upstream flow path. Nevertheless, the resulting backpressure increase was only 5% at the end of the run.

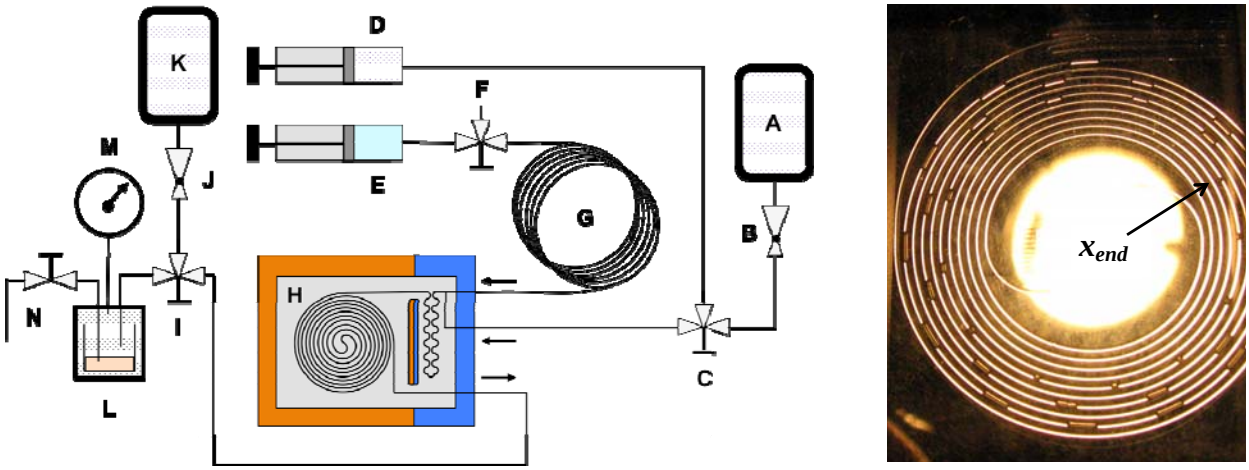

Figure 1. *Left:* Setup for the autoxidation experiments. (A) Oxygen cylinder, (B) reduction valve, (C) 3-way valve, (D) oxygen syringe, (E) water-filled liquid syringe, (F) refill port, (G) 1/16" PFA reservoir for liquid substrate, (H) Si/SiO_2/pyrex microreactor with cooled inlet zone, incl. mixing section(blue), heated reaction zone, spiral channel (orange) and insulation gap between these two zones, (I) split valve, (J) reduction valve, (K) nitrogen cylinder. *Right:* Live reactor, the point of gas exhaustion labelled with x_{end}.

Kinetics

Since the experiments were performed under continuous flow conditions, the concentration at a given point in the reactor was time-independent, i.e. in steady-state. This was exploited to obtain kinetic data: The disappearance point of the gas bubbles (x_{end}) was taken as a robust measure for the time of full gas consumption, analogous to the H_2 bubble shrinkage used by Bakker et al.[44] to determine hydrogenation kinetics. After two residence times for equilibration, the x_{end} values were read out visually (Figure 1, right), using a calibrated internal coordinate scale (see Supporting Information), and averaged over at least three readings. From that data, knowing the superficial flow rates of the two phases and the rate law of the chemical reaction, the effective reaction rate constant was obtained using equation 1,

$$k_{eff} = \sqrt{\frac{\alpha\gamma}{\beta}\frac{p(O_2)}{RT}}\, 2\mathrm{LFR}_{\mathrm{sup}}\frac{1+2/3\,\gamma}{x_{end}}[\mathrm{RH}]^{-3/2} \qquad (1)$$

where α (average O_2 incorporation per product molecule) and β (average probability of a primary product being hydroperoxide) are substrate-specific parameters, γ is the gas-to-liquid slug ratio, $p(O_2)$ is the oxygen pressure, LFR_{sup} the superficial liquid flow rate, x_{end} the bubble-end-point and [RH] the substrate concentration. This formula is valid for all substrate-assisted peroxide initiation mechanisms, e.g. olefins.[45] Equation 1 is derived in the Supporting Information. Physically, the effective rate constant is composed of three components, representing chain initiation, propagation and termination, specifically:

$$r_{eff} = k_{prop}\left[\mathrm{ROO}^{\bullet}\right][\mathrm{RH}] = k_{prop}\sqrt{\frac{k_{init}[\mathrm{RH}][\mathrm{ROOH}]}{k_{term}}}[\mathrm{RH}] = k_{eff}[\mathrm{ROOH}]^{1/2}[\mathrm{RH}]^{3/2} \qquad (2)$$

In order to evaluate the temperature-dependency of the effective rate constants, we generated Arrhenius plots. The preexponential prefactor is susceptible to all parameters of Equation 1 whereas the activation energy depends only on the robust, direct experimental quantity x_{end} as follows.

$$E_A = -R\frac{\partial \ln(k_{eff})}{\partial\left(1/T\right)} = -R\frac{\partial \ln\left(1/x_{end}\right)}{\partial\left(1/T\right)} \tag{3}$$

An extension of this claim for other mechanisms such as product-assisted initiation mechanisms (e.g. cyclohexane)[45] and non-autocatalytic oxidations (e.g. aldehyde)[46] is given in the Supporting Information. To obtain the gas-liquid mass-transfer value (k_La), the intrinsic chemical rate (Eq. 2) was equated to the maximum mass transfer rate, i.e. the product of k_La and the saturated oxygen concentration, which was obtained from Henry's law (H(**1**) = 0.030 M bar^{-1}).[47]

Experiments

Organic substrates were purchased from Sigma-Aldrich in 99% purity (**1**) or 65% purity (**9**, nominal minimum value, the effective purity of this lot was 80%), respectively. In order to avoid effects related to high pressures, **1** was given preference over its regioisomer α-pinene in the present study.[47] The technical grade quality of **9** was chosen to obtain data for (economically) feasible conditions for potential scale-up of this chemistry: Whereas **1** can be purchased inexpensively in high purity, there is a massive cost increase for obtaining **9** in analytical grade, caused by the above-mentioned origin of the feedstock (i.e. renewable resource). Oxygen gas

was given preference over pressurized air, in order to make it possible to monitor the reaction online via the full disappearance of gas phase. Gas chromatography (GC-FID, HP-5MS column, 30 m × 320 μm × 0.25 μm, samples internally standardized with biphenyl) was used to quantify selectivity and mass balance in the autoxidation of **9** to **10**. Reductive sample preparation (adding a 5-fold excess of triphenylphosphine) was applied to deactivate intermediate hydroperoxides, which could else give an artificially high signal of **10** due to thermal rearrangement in the injection chamber. For the autoxidation of **1**, the observed product mixture did not significantly differ from the one published previously.[17]

Computations

Quantum mechanical calculations were at the UB3LYP/6-311++G(df,pd)//UB3LYP/6-31G(d,p) level of theory,[48] as previously validated against correlated methods, for radical oxidation reactions.[49] All single-point energies were zero-point corrected. In the text, we simply refer to this technique by "DFT". Calculations were performed using Gaussian 03 (tight SCF convergence criteria were chosen),[50] visualizations were done using Avogadro 1.1.0[51] and QuteMol 2.8.3.[52]

RESULTS AND DISCUSSION

Calibration with β-Pinene

Under the chosen harsh reaction conditions, autoxidation of β-pinene (**1**) and concomitant consumption of oxygen occurred spontaneously without the need for initiating agents or catalysts. The reaction end point (x_{end}) could be quantitatively measured, as described in the Experimental Section. We studied x_{end} as a function of temperature and liquid flow rate (Figure 2A). As expected, increasing temperature and decreasing flow rate led to shorter x_{end} values. The precise residence times (t_{res}) are different for every set of conditions, since the flow rate is not constant within the reactor. Nevertheless, to give a range, t_{res} varied roughly between 1-5 min. Under the conditions used, conversion of **1** was limited to 5%, due to full gas consumption. In principle, higher conversions can be achieved by either working with higher oxygen pressures, by altering the gas-liquid composition (e.g. by working in a packed bed reactor or scaling up into a Corning® advanced flow reactor), or by repeating multiple oxidation runs in series (see section on valencene oxidation). Effective rate constants (k_{eff}) were then obtained by application of equation 1 (Figure 2B). For covering the broadest temperature range possible, the upper six values were obtained from the 60 μL/min data, whereas the lower six values were obtained from the 15 μL/min data. Good consistency for both flow rates was found, as expected from the flow-independent chemical quantity k_{eff}.

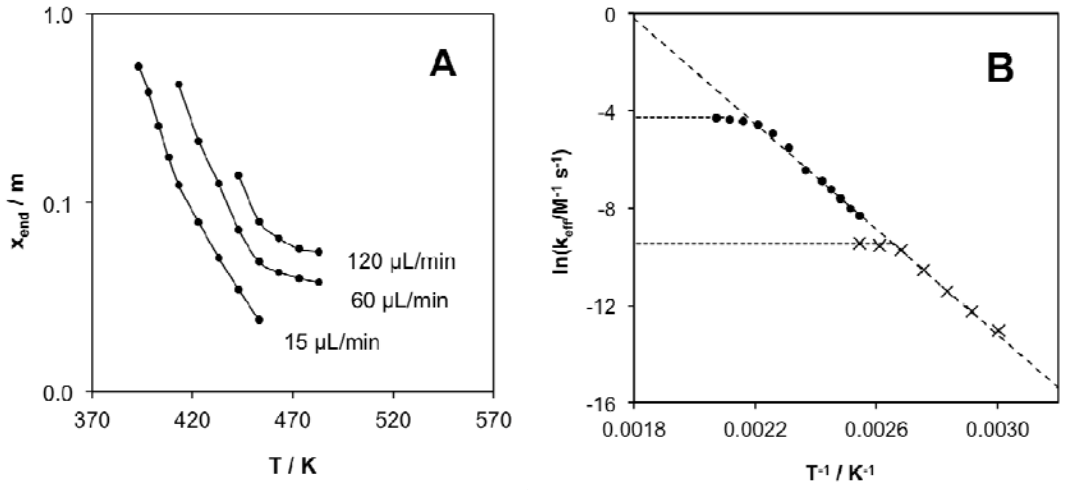

Figure 2. Autoxidation of **1**. (A) x_{end} as a function of temperature and liquid flow rate ($p(O_2)$ = 200 psi), plotted on a logarithmic scale. (B) Arrhenius plot. The microreactor data from this study (circles; 15 – 60 µL/min, $\alpha = 0.77$, $\beta = 0.4$, $\gamma = 0.6$) is shown along with the data from an earlier study in batch (crosses; bubble column).[17] The dashed line indicates intrinsic kinetics ($E_{A,eff}$ = 21.6 kcal mol^{-1}; $A_{eff} = 2.5 \times 10^8$ M^{-1} s^{-1}). The mass transfer limits (denoted with dotted lines) are reached at $k_La = 0.15$ s^{-1} and 0.009 s^{-1}, for microreactor and batch, respectively.

The intrinsic kinetics found for this oxidation system, i.e. activation energy and exponential prefactor, are in very good agreement with the data from our earlier batch study (Figure 2B).[17] This indicates that kinetic data for autoxidations, obtained with microreactors, can be used as a solid basis for scaling up processes in larger flow reactors or even in batch. This is particularly useful, since obtaining kinetic data in batch or large flow-reactors is significantly more labor and material intensive. Also, the safety situation is difficult to assess beforehand, when the kinetic data is still unknown. Thus, non-hazardous screening of experimental conditions as well as determination of kinetic data in the microreactor is clearly preferred, even if the eventual goal is

to run the process in another reactor type. Furthermore, with the presented flow setup we are able to operate at higher temperatures because of the enhanced mass transfer resulting from both a higher gas-liquid k_La value (0.15 s^{-1} vs. 0.009 s^{-1} in batch) and a higher concentration of oxygen at the higher pressure (13 atm in the microreactor vs. 1 atm in batch). Overall, the process can thus be intensified by more than two orders of magnitude. Note that the microreactor's k_La value, as obtained from this study, is in good agreement with the 0.1 s^{-1} value obtained in previous reactor characterization[15] (CO_2/H_2O system, extrapolated to 15 mm s^{-1} superficial flow rate), which further supports the quantitative validity of our data.

Application to Valencene

Using the same procedure as described above, the autoxidation kinetics of **9** were measured (Figure 3). A slightly lower k_La value than in the case of **1** was found. However, for the determination of this value, an identical Henry constant for solubility of oxygen in **9** (as in **1)** was assumed, due to the lack of actual reference data. This might be a somewhat erroneous overestimation, such that the reported k_La value would be underestimated accordingly. Nevertheless, the order of magnitude seems reasonable. Concerning the absolute value of the found Arrhenius parameters, note that direct comparison of with other substrates is not recommended and some caution is required with interpretation. The reason for this is that the starting material had a purity of only 65% (see Experimental Section), with the impurities being at least as reactive as **9**. Indeed, the concentration of the impurities decreased parallel with the concentration of **9**, during autoxidation, and the impact of the impurities on the precise values of the kinetic parameters is likely to be non-negligible (chain reaction are notoriously influenced by impurities).[53] However, if **9** in this technical quality is used as the feedstock, the kinetic

parameters do have the reported values. Those values then do not only lump together different elementary reaction steps but also account for the contributions of the different substrates in the mixture. Since the intrinsic kinetics are valid across different reactors (see above, Figure 2), these data should be useful for a controlled, safe scale-up of this chemistry to larger flow reactors or even to batch.

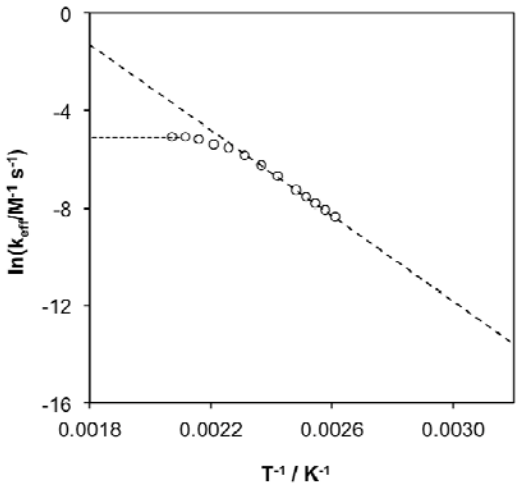

Figure 3. Arrhenius plot for autoxidation of **9** (empty circles, $p(O_2)$ = 200 psi, 15 – 30 µL/min, α = 0.85, β = 0.7, γ = 1.0). The dashed line indicates intrinsic kinetics ($E_{A,eff}$ = 17.5 kcal mol^{-1}; A_{eff} = 2 × 10^6 M^{-1} s^{-1}). The dotted line indicates mass transfer limit (k_La = 0.10 s^{-1}).

With regard to selectivity, at first sight **9** does not seem to be an ideal candidate for radical-based oxidations, since there are two double bonds in the molecule and based on a first-order structure-activity based estimation, eight carbon centers are "equally" reactive (Scheme 2).[22] Even worse, functionalization of position 8 seems to be favored over the desired position 3, due to the tertiary C-H bond. However, stereoelectronic conformation effects are known to play a major role in fine-tuning the selectivity of cyclic olefins.[54,55] Thus, we performed a more reliable

selectivity estimation using DFT. The results were very promising, both regarding chemo- and regioselectivity (Table 1). Since the intermediate allyl radical (that forms upon H abstraction) is identical for both cases, functionalization of both 3 *cis* and 3 *trans* positions leads to the desired product and the selectivity values can be cumulated, yielding an overall prediction of 66% selectivity towards oxyfunctionalization at the desired position.

Table 1. DFT predictions for chemo- and regioselectivity towards functionalization of **9** with a model peroxyl radical, i.e. *i*PrOO$^{\bullet}$. Activation energies (E_A) and selectivities (S) are at 180°C. Identical exponential prefactors are assumed. For computational details see Materials and Methods section.

elementary reaction	E_A [kcal mol^{-1}]	S [%]
C=C addition, 2 *cis* (*trans*)	13.49 (18.44)	4 (0)
H abstraction, 3 *trans* (*cis*)	11.10 (13.58)	62 (4)
H abstraction, 8 *cis*	12.67	11
H abstraction, 10 *cis* (*trans*)	12.49 (19.66)	13 (0)
C=C addition, 12	13.39	5
H abstraction, 13	14.86	1

Although there appears to be no systematic autoxidation study of **9** to **10**, there is a report by Davies,[43] where he described slow autoxidation of **9** to the intermediate hydroperoxides at room temperature (90 h) using hyponitrite as a radical initiator and $CHCl_3$ as solvent. In this study, formation of the corresponding nootkatyl hydroperoxide, i.e. $R_{(3)}OOH$, was reported, whereas no isomeric hydroperoxide ($R_{(1)}OOH$) was found. Moreover, in the product mixture, Davies

observed a *cis* to *trans* ratio of 1:5.6 (at 25°C), revealing a ~1 kcal/mol more stable *trans*-$R_{(3)}OOH$. Our DFT results, predicting *trans*-$R_{(3)}OOH$ to be more stable than *cis*-$R_{(3)}OOH$ by 0.7 kcal mol^{-1}, as well as more stable than *trans*-$R_{(1)}OOH$ by 6.7 kcal mol^{-1} and *cis*-$R_{(1)}OOH$ by 9.2 kcal mol^{-1}, are in perfect agreement with these observations. Note that for such allylic hydroperoxide intermediates, the (implicit) assumption of a thermodynamically controlled isomer distribution is valid, since they can dynamically undergo Smith epimerization (via peroxyl redissociation) and Schenck rearrangement (via peroxyl 2,3-shifts) in the presence of radicals.[43]

Inspired by our earlier observation in pinene oxidation,[17,47] where overoxidation of hydroperoxides **2** and **3** efficiently yields carbonyls **6** and **7**, respectively, as secondary reaction products, we hypothesized that the same might be happening in the case $R_{(3)}OOH$, yielding **10**. In order to test this hypothesis with our microreactor setup, we carried out a sequence of ten autoxidation runs (using a batchwise recycle mode), where each run incrementally raised the overall conversion. The results are given in Figure 4. For reporting of results, a three-parameter formalism was given preference over the conventional two-parameter formalism (where apparent selectivity and mass balance are combined into one parameter, the true selectivity) in order to allow for a more meaningful comparison of our results with other studies published (see below). Equation (4) shows how the variables are connected, with *Y* being the yield [mol nootkatone produced per initial mol valencene], *C* the conversion [mol valencene reacted per initial mol valencene], *S* the apparent selectivity [mol nootkatone produced per mol products observed] and *MB* the mass balance [mol products observed per mol valencene reacted].

$$Y = C \cdot S \cdot MB \qquad (4)$$

The residence time was about 2 minutes in each run, totaling to 20 minutes overall residence time. A steady increase in the conversion could be observed, slightly flattening off at high conversions. The mass balance was constant throughout the runs and amounted to about 35%. The reason of the low GC mass balance, i.e. why roughly two thirds of the reaction products end up being non-volatile, is unclear and it can only be speculated to why this happens. A plausible explanation would be that in this radical-dominated system, to some extent radical polymerization would be initiated at the olefin functional groups, and although Table 1 suggests this would occur to only ~9% (lines 1 and 5), subsequent oligomerization could potentially lead to significant consumption of substrate. In any case, fact is that the mass balance for all nine studies presented in Table 2 is consistently low, with a mean value of only 50%. Thus, the results presented herein are not unexpected in this regard.

The apparent product selectivity increased in the first couple of runs from 20 to about 40%. This can be understood by the above-mentioned overoxidation effect: The hydroperoxide intermediates (ROOH) are more easily oxidized than their parent hydrocarbons, the product of such an overoxidation event being ketone. The yield increased by about 1% per run, reaching 10% after the series of runs. From this, it can be concluded that allylic hydroperoxides must indeed form a significant fraction in the primary product distribution. Beside nootkatone, that was the single major product, a large array of mostly unresolved oxidation products was also found. Among them, the allylic alcohols (nootkatols), originating in part from allylic hydroperoxide reduction in the sample workup step, was roughly 10%, showing that the optimization potential by a follow-up oxidation of nootkatyl-O(O)H species to nootkatone would be very limited.

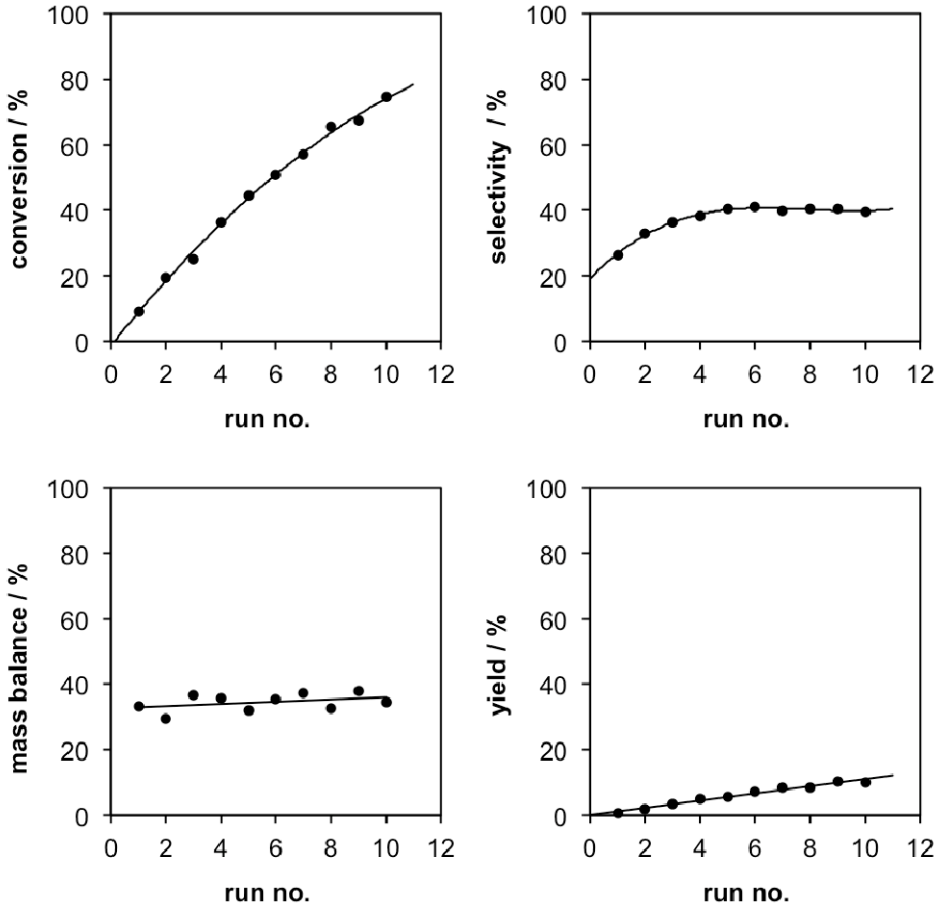

Figure 4. Autoxidation of **9**. Conversion is based on reacted substrate (including impurities), selectivity is based on all volatile products, mass balance accounts for the fraction of volatile products among all products, yield refers to starting amount of substrate.

In terms of downstream processing, it has been shown that **9** can be separated from the product mixture and recycled, via a selective sorption approach.[32] Probably, the product mixture can be used directly, as such, since the other oxidation products have similar organoleptic characteristics, yet with a much higher odor threshold.[56] Therefore, the odor interference in the end product might be small. Care should be taken, however, in that the remaining traces of hydroperoxide in the product mixture must be reduced before putting the product mixture into an

end-user commodity.[57] In the present case, we performed such reduction with triphenylphosphine, other more food-compatible reducing agents include sodium thiosulfate or ascorbic acid.

Although higher yields have been reported in biotechnological approaches, it is not impossible that the present, chemical process might be beneficial under certain circumstances. For instance, in view of the increasing availability of **9** (see above), prices are expected to decrease very significantly on a relatively short term. As a consequence, it might be the case that the cost-determining step will shift from purchasing **9** as raw material to producing **10** in an effective way, i.e. factors such as lowering costs for aqueous waste disposal and increasing space-time yield of **10** must be considered. In this regard, it could be worthwhile to sacrifice some selectivity, when the space-time yield is dramatically increased in return. Indeed, our observed space-time yield is approximately 0.3 kg of **10** per liter reactor volume per hour, which is 3–6 orders of magnitude higher than the biotechnological state-of-the-art (see Table 2 for a benchmark). Consequently, with a much smaller footprint, comparable production rates can be achieved. Moreover, there is no need for genetically modified cell cultures or enzymes, and the cost-intensive workup of large aqueous waste streams can be avoided. All this must be acknowledged when making an overall cost estimation, and it could not be excluded that the net cost of such a high temperature oxidation process in flow would be competitive with the above presented biotech processes. A further advantage of the present method is that it does not depend on any chemical auxiliaries, solvents or catalysts, simplifying the regulatory approval procedure required for food applications.

Table 2. Compilation of existing biotechnological processes, benchmarked to our chemical process. *S* = apparent selectivity; *C* = conversion; *MB* = mass balance; *Y* = yield; *STY* = space-time yield.

Process	*S* [%]	*C* [%]	*MB* [%][b)]	*Y* [%]	*STY* [g L^{-1} h^{-1}]
this paper	40	75	35	10	316
Drawert[33] (1984)	97[a)]	95	67	62[a)]	0.0001
Muller[32] (1998)	42[a)]	86	89	32[a)]	0.2
Huang[36] (2001)	43	66	100	29	0.03
Kaspera[37] (2005)	52	80	11	5	0.0001
Fraatz[58] (2009)	76[a)]	60	41	19[a)]	0.01
Krügener[59] (2010)	28	100	50[c)]	14	0.02
Zorn[60] (2012)	67[a)]	70[d)]	10[d)]	5[a)]	0.01
Rickert[38] (2012)	62[a)]	94	48	28[a)]	0.01

a) Intermediate hydroperoxide not taken into account.

b) Estimated from available data, where not given explicitly.

c) Estimated based on TLC results.

d) Estimation based on fed-batch transformation.

Although our process is attractive in terms of space-time yield, the yield is about five times lower than in the biotechnological state-of-the-art. However, this is a conservative comparison, since in some works, hydroperoxide dehydration was not prevented in the GC analyses (i.e. no chemical reduction prior to analysis), which can lead to an artificially enhanced signal of **10** in the chromatogram. Indeed, the reports taking care of (intermediate) hydroperoxides report an average of 14.5% yield, which seems to be more realistic than the average 29.2% yield, reported by the other reports (denoted by [a)] in Table 2). This point was mentioned already by Krügener.[59]

CONCLUSION

In summary, we have described a microfluidic setup able to safely and continuously perform the oxyfunctionalization of olefins at rates that are two orders of magnitude faster than conventional batch procedures. The acceleration was due to process intensification by increased temperature made possible by the favorable combination of a fast gas-liquid mass transfer constant with elevated system pressures. The reactions were carried out solvent-free to prevent solvent cooxidation. Since the reactor operates in a steady-state mode, visual access to the biphasic reaction enabled measurements of reaction kinetics by determining the end position of the gas bubbles within the reaction channel. The developed system was calibrated with the well-known β-pinene autoxidation system and was then applied to the synthetically interesting transformation of (+)-valencene to (+)-nootkatone. For the latter, a moderate yield could be obtained; yet, the space-time yield was better by at least three orders of magnitude, compared to the established biotechnology approaches.

ASSOCIATED CONTENT

Supporting Information. Derivation of equations, experimental details. This material is available free of charge via the Internet at http://pubs.acs.org.

AUTHOR INFORMATION

Corresponding Author

*Email: kfjensen@mit.edu

ACKNOWLEDGMENTS

The authors acknowledge the financial support from the Swiss National Science Foundation (SNF) and Novartis–MIT Center for Continuous Manufacturing. Prof. S. L. Buchwald is acknowledged for providing computational resources.

REFERENCES

(1) Fortt, R.; Wootton, R. C. R.; de Mello, A. J. Continuous-Flow Generation of Anhydrous Diazonium Species: Monolithic Microfluidic Reactors for the Chemistry of Unstable Intermediates. *Org. Process Res. Dev.* **2003**, *7*, 762-768.

(2) Jaenisch, K.; Baerns, M.; Hessel, V.; Ehrfeld, W.; Haverkamp, V.; Loewe, H.; Wille, C.; Guber, A. Direct, fluorination of toluene using elemental fluorine in gas/liquid microreactors. *J. Fluorine Chem.* **2000**, *105*, 117-128.

(3) Koos, P.; Gross, U.; Polyzos, A.; O'Brien, M.; Baxendale, I.; Ley, S. V. Teflon AF-2400 mediated gas–liquid contact in continuous flow methoxycarbonylations and in-line FTIR measurement of CO concentration. *Org. Biomol. Chem.* **2011**, *9*, 6903-6908.

(4) Hartman, R. L.; McMullen, J. P.; Jensen, K. F. Deciding Whether To Go with the Flow: Evaluating the Merits of Flow Reactors for Synthesis. *Angew. Chem. Int. Ed.* **2011**, *50*, 7502-7519.

(5) Hartman, R. L.; Jensen, K. F. Microchemical systems for continuous-flow synthesis. *Lab Chip* **2009**, *9*, 2495-2507.

(6) Calabrese, G. S.; Pissavini, S. From batch to continuous flow processing in chemicals manufacturing. *AIChE J.* **2011**, *57*, 828-834.

(7) Hartman, R. L.; Sahoo, H. R.; Yen, B. C.; Jensen, K. F. Distillation in microchemical systems using capillary forces and segmented flow. *Lab Chip* **2009**, *9*, 1843-1849.

(8) Hartman, R. L.; Naber, J. R.; Buchwald, S. L.; Jensen, K. F. Multistep Microchemical Synthesis Enabled by Microfluidic Distillation. *Angew. Chem. Int Ed.* **2010**, *49*, 899-903.

(9) Noël, T.; Kuhn, S.; Musacchio, A. J.; Jensen, K. F.; Buchwald, S. L. Suzuki–Miyaura Cross□Coupling Reactions in Flow: Multistep Synthesis Enabled by a Microfluidic Extraction. *Angew. Chem. Int. Ed.* **2011**, *50*, 5943-5946.

(10) Smith, C. J.; Nikbin, N.; Ley, S. L.; Lange, H.; Baxendale, I. R. A fully automated, multistep flow synthesis of 5-amino-4-cyano-1,2,3-triazoles. *Org. Biomol. Chem.* **2011**, *9*, 1938-1947.

(11) Hermans, I.; Spier, E. S.; Neuenschwander, U.; Turrà, N.; Baiker, A. Selective oxidation catalysis: opportunities and challenges. *Top. Catal.* **2009**, *52*, 1162-1174.

(12) Zaborenko, N. *Continuous-flow study and scale-up of conventionally difficult chemical processes.* PhD Thesis Mass. Inst. Technol., Cambridge, 2010.

(13) Bedore, M. W.; Zaborenko, N.; Jensen, K. F.; Jamison, T. F. Aminolysis of Epoxides in a Microreactor System: A Continuous Flow Approach to β-Amino Alcohols. *Org. Process Res. Dev.* **2010**, *14*, 432-440.

(14) Marre, S.; Adamo, A.; Basak, S; Aymonier, C.; Jensen, K.F. Design and packaging of microreactors for high pressure and high temperature applications. *Ind. Eng. Chem. Res*. **2010**, *49*, 11310–11320.

(15) Kuhn, S.; Jensen, K. F. A pH-Sensitive Laser-Induced Fluorescence Technique To Monitor Mass Transfer in Multiphase Flows in Microfluidic Devices. *Ind. Eng. Chem. Res.* **2012**, *51*, 8999-9006.

(16) Gscheidmeier, M.; Fleig, H. *Turpentines*. In Ullmann′s Encyclopedia of Industrial Chemistry, Wiley-VCH, Weinheim, 2005.

(17) Neuenschwander, U.; Meier, E.; Hermans, I. Peculiarities of β−Pinene Autoxidation. *ChemSusChem* **2011**, *4*, 1613-1621.

(18) Crowe, T. D.; White, P. J. Adaptation of the AOCS official method for measuring hydroperoxides from small-scale oil samples. *J. Am. Oil Chem. Soc.* **2001**, *78*, 1267-1269.

(19) Fahlbusch, K. G.; Hammerschmitdt, F. J.; Panten, J.; Pickenhaben, W.; Schatkowski, D. *Flavors and Fragrances*. In Ullmann′s Encyclopedia of Industrial Chemistry, Wiley-VCH, Weinheim, 2005.

(20) Mallat, T.; Baiker, A. Reactions in "sacrificial" solvents. *Cat. Sci. Technol.* **2011**, *1*, 1572-1583.

(21) Neuenschwander, U.; Hermans, I. Thermal and catalytic formation of radicals during autoxidation. *J. Catal.* **2011**, *287*, 1-4.

(22) Franz, G.; Sheldon, R. A. *Oxidation*. In Ullmann's Encyclopedia of Industrial Chemistry, Wiley-VCH, Weinheim, 2000.

(23) Nisperos-Carriedo, M. O.; Shaw, P. E. n of volatile flavor components in fresh and processed orange juices. *J. Agric. Food Chem.* **1990**, *38*, 1048-1052.

(24) S. Kotachi, J. Ueda, S. Tanaka, US Patent 7'235'275 B2, June 26, 2007.

(25) Liat, S.-A.; Shalit, M.; Frydman, A.; Bar, E.; Holland, D.; Or, E.; Lavi, U.; Lewinsohn, E.; Eyal, Y. Citrus fruit flavor and aroma biosynthesis: isolation, functional characterization, and developmental regulation of Cstps1, a key gene in the production of the sesquiterpene aroma compound valencene. *Plant J.* **2003**, *36*, 664-674.

(26) Chappell, J.; Greenhagen, B. US Patent 2006/0218661 A1, Sep. 28, 2006.

(27) As advertised on their company websites: www.allylix.com; www.isobionics.com.

(28) Berry, R. E.; Wagner, C. J.; Moshonas, M. G. Flavor studies of nootkatone in grapefruit juice. *Food Sci.* **2006**, *32*, 75-78.

(29) Wilson, C. W. III; Shaw, P. E. Synthesis of Nootkatone from Valencene. *J. Agric. Food Chem.* **1978**, *26*, 1430-1432.

(30) Moshonas, M. G.; Shaw, P. E. Analysis of volatile flavor constituents from grapefruit essence. *J. Agric. Food Chem.* **1971**, *19*, 119-120.

(31) Fraatz, M. A.; Berger, R. G.; Zorn, H. Nootkatone, a biotechnological challenge. *Appl. Microbiol. Biotechnol.* **2009**, *83*, 35-41.

(32) Muller, B.; Dean, C.; Schmidt, C.; Kuhn, J.-C. US Patent 5'847'226, Dec. 8, 1998.

(33) Drawert, F.; Berger, R. G.; Godelmann, R. Regioselective biotransformation of valencene in cell suspension cultures of citrus sp. *Plant Cell Reports* **1984**, *3*, 37-40.

(34) Ishida, T. Biotransformation of Terpenoids by Mammals, Microorganisms, and Plant-Cultured Cells. *Chem. Biodivers.* **2005**, *2*, 569-590.

(35) Sowden, R. J.; Yasmin, S.; Rees, N. H.; Bell, S. G.; Wong, L.-L. Biotransformation of the sesquiterpene (+)-valencene by cytochrome P450cam and P450BM-3. *Org. Biomol. Chem.* **2005**, *3*, 57-64.

(36) Huang, R.; Christenson, P. A.; Labuda, I. M. US Patent 6'200'786 B1, Mar. 13, 2001.

(37) Kaspera, R.; Krings, U.; Nanzad, T.; Berger, R. G. Bioconversion of (+)-valencene in submerged cultures of the ascomycete Chaetomium globosum. *Appl. Microbiol. Biotechnol.* **2005**, *67*, 477-483.

(38) Rickert, A.; Krombach, V.; Hamers, O.; Zorn, H.; Maison, W. Enzymatic allylic oxidations with a lyophilisate of the edible fungus Pleurotus sapidus. *Green Chem.* **2012**, *14*, 639-644.

(39) Hunter, G. L. K.; Brogden, W. B. Conversion of valencene to nootkatone. *J. Food Sci.* **1965**, *30*, 876-878.

(40) Salvador, J. A. R.; Clark, J. H. The allylic oxidation of unsaturated steroids by tert-butyl hydroperoxide using surface functionalised silica supported metal catalysts. *Green Chem.* **2002**, *4*, 352-356.

(41) Silvestre, S. M.; Salvador, J. A. R.;Allylic and benzylic oxidation reactions with sodium chlorite. *Tetrahedron* **2007**, *63*, 2439-2445.

(42) Salvador, J. A. R.; Silvestre, S. M.; Pinto, R. M. A. Bismuth(III) Reagents in Steroid and Terpene Chemistry. *Molecules* **2011**, *16*, 2884-2913.

(43) Davies, A. G.; Davison, I. G. E. The rearrangements of allylic hydroperoxides derived from (+)-valencene. *J. Chem. Soc. Perkin Trans. II* **1989**, 825-830.

(44) Bakker, J. J. W.; Zieverink, M. M. P.; Reintjens, R. W. E. G; Kapteijn, F.; Moulijn, J. A.; Kreutzer, M. T. Heterogeneously catalyzed continuous-flow hydrogenation using segmented flow in capillary columns. *ChemCatChem* **2011**, *3*, 1155 – 1157.

(45) In the case of alkanes, e.g. cyclohexane, the situation is slightly different: There, the carbonyl product was found to further assist peroxide initiation, since the alkane itself is very inert. See: Hermans, I.; Jacobs, P. A.; Peeters, J. Understanding the Autoxidation of Hydrocarbons at the Molecular Level and the Consequences for Catalysis. *J. Mol. Cat. A* **2006**, *251*, 221-228.

(46) Neuenschwander, U.; Neuenschwander, J.; Hermans, I. Cavitation-Induced Radical-Chain Oxidation of Valeric Aldehyde. *Ultrason. Sonochem.* **2012**, *19*, 1011-1014.

(47) Neuenschwander, U.; Hermans, I. Autoxidation of alpha-Pinene at High Oxygen Pressure. *Phys. Chem. Chem. Phys.* **2010**, *12*, 10542-10549.

(48) Becke, A. D. *J. Chem. Phys.* **1993**, *98*, 5648-5652.

(49) Hermans, I.; Nguyen, T. L.; Jacobs, P. A.; Peeters, J. Autoxidation of Cyclohexane: Conventional Views Challenged by Theory and Experiment. *ChemPhysChem* **2005**, *6*, 637-645.

(50) Gaussian 03, Revision B.03, M. J. Frisch, G. W. Trucks, H. B. Schlegel, G. E. Scuseria, M. A. Robb, J. R. Cheeseman, J. A. Montgomery, Jr., T. Vreven, K. N. Kudin, J. C. Burant, J. M. Millam, S. S. Iyengar, J. Tomasi, V. Barone, B. Mennucci, M. Cossi, G. Scalmani, N. Rega, G. A. Petersson, H. Nakatsuji, M. Hada, M. Ehara, K. Toyota, R. Fukuda, J. Hasegawa, M. Ishida, T. Nakajima, Y. Honda, O. Kitao, H.

Nakai, M. Klene, X. Li, J. E. Knox, H. P. Hratchian, J. B. Cross, V. Bakken, C. Adamo, J. Jaramillo, R. Gomperts, R. E. Stratmann, O. Yazyev, A. J. Austin, R. Cammi, C. Pomelli, J. W. Ochterski, P. Y. Ayala, K. Morokuma, G. A. Voth, P. Salvador, J. J. Dannenberg, V. G. Zakrzewski, S. Dapprich, A. D. Daniels, M. C. Strain, O. Farkas, D. K. Malick, A. D. Rabuck, K. Raghavachari, J. B. Foresman, J. V. Ortiz, Q. Cui, A. G. Baboul, S. Clifford, J. Cioslowski, B. B. Stefanov, G. Liu, A. Liashenko, P. Piskorz, I. Komaromi, R. L. Martin, D. J. Fox, T. Keith, M. A. Al-Laham, C. Y. Peng, A. Nanayakkara, M. Challacombe, P. M. W. Gill, B. Johnson, W. Chen, M. W. Wong, C. Gonzalez, J. A. Pople, Gaussian, Inc., Wallingford CT, 2004.

(51) Hanwell, M. D.; Curtis, D. E.; Lonie, D. C.; Vandermeersch, T.; Zurek, E.; Hutchison, G. R. Avogadro: An advanced semantic chemical editor, visualization, and analysis platform. *J. Cheminformatics* **2012**, *4*, 17.

(52) Tarini, M.; Cignoni, P.; Montani, C. Ambient Occlusion and Edge Cueing for Enhancing Real Time Molecular Visualization. *IEEE Transactions on Visualization and Computer Graphics* **2006**, *12*, 1237-1244.

(53) Hermans, I.; Peeters, J.; Jacobs, P. A. Enhanced Activity and Selectivity in Cyclohexane Autoxidation by Inert H-Bond Acceptor Catalysts. *ChemPhysChem* **2006**, *7*, 1142-1148.

(54) Neuenschwander, U.; Czarniecki, B.; Hermans, I. The Conformations of Cyclooctene: Consequences for Epoxidation Chemistry. *Journal of Organic Chemistry* **2011**, *76*, 10236-10240.

(55) Neuenschwander, U.; Czarniecki, B.; Hermans, I. The Origin of Regioselectivity in Humulene Functionalization. *Journal of Organic Chemistry* **2012**, *77*, 2865-2869.

(56) Shaw, P. E.; Wilson, C. W. III. *Importance of Selected Volatile Components to Natural Orange, Grapefruit, Tangerine, and Mandarin Flavors.* In Citrus Nutrition and Quality, chapter 9, Ed. Nagy, S. ACS Symposium Series, Washington DC, 1980.

(57) Matura, M.; Sköld, M.; Börje, A.; Andersen, K. E.; Bruze, M.; Frosch, P.; Goossens, A.; Johansen, J. D.; Svedman, C.; White, I. R.; Karlberg, A. T. *Contact Dermatitis* **2005**, *52*, 320-328.

(58) Fraatz, M. A.; Riemer, S. J. L.; Stöber, R.; Kaspera, R.; Nimtz, M.; Berger, R. G.; Zorn, H. A novel oxygenase from Pleurotus sapidus transforms valencene to nootkatone. *J. Mol. Cat. B* **2009**, *61*, 202-207.

(59) Krügener, S.; Krings, U.; Zorn, H.; Berger, R. G. A dioxygenase of Pleurotus sapidus transforms (+)-valencene regio-specifically to (+)-nootkatone via a stereo-specific allylic hydroperoxidation. *Biores. Technol.* **2010**, *101*, 457-462.

(60) Rickert, A.; Krombach, V.; Hamers, O.; Zorn, H.; Maison, W. Enzymatic allylic oxidations with a lyophilisate of the edible fungus Pleurotus sapidus. *Green Chem.* **2012**, *14*, 639-644.

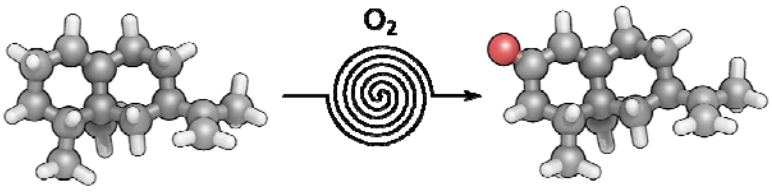

Supporting Information

Olefin Autoxidation in Flow

*Ulrich Neuenschwander, Klavs F. Jensen**

Department of Chemical Engineering,
Massachusetts Institute of Technology,
77 Massachusetts Avenue, Cambridge MA 02139, USA.

*kfjensen@mit.edu

CONTENTS

Derivation of equation 1

Substrate-assisted initiation mechanisms

The effective rate of the autoxidation reaction is:

$$r_{eff} = k_{prop}\left[\mathrm{ROO^{\cdot}}\right]\left[\mathrm{RH}\right] = k_{prop}\sqrt{\frac{k_{init}\left[\mathrm{RH}\right]\left[\mathrm{ROOH}\right]}{k_{term}}}\left[\mathrm{RH}\right] = k_{eff}\left[\mathrm{ROOH}\right]^{1/2}\left[\mathrm{RH}\right]^{3/2} \tag{2}$$

Let us define the sum of all oxidation products, as a function of time, as follows:

$$P(t) = \sum_i P_i(t)$$

The crucial point is to couple the differential equations of oxygen consumption and product formation:

$$-\left(\frac{d[\mathrm{O_2}]_{liq}}{dt}\right)_{\text{reaction}} = \alpha\frac{d[\mathrm{P}]_{liq}}{dt} = \frac{\alpha}{\beta}\frac{d[\mathrm{ROOH}]_{liq}}{dt} \tag{S1}$$

In this equation, α refers to the amount of oxygen incorporation into the products ("How many oxygen molecules are needed to form an average product molecule P?") and β refers to the fraction of autocatalytically active hydroperoxide molecules (ROOH) within the products ("How likely is it for a product molecule to be a hydroperoxide?").

With the continuous replacement of oxygen reacted in the liquid phase by mass transfer from the gas phase to the liquid phase, we can assume steady-state:

$$\left(\frac{d[\mathrm{O_2}]_{liq}}{dt}\right)_{\text{total}} = 0$$

and thus

$$-\left(\frac{d[\mathrm{O_2}]_{liq}}{dt}\right)_{\text{reaction}} = \left(\frac{d[\mathrm{O_2}]_{liq}}{dt}\right)_{\text{mass transfer}}$$

Of course, this assumption only holds for non-mass-transfer-limited conditions, where intrinsic kinetics are dominant. By substituting the above into Eq. S1, we obtain:

$$\left(\frac{d[\mathrm{O_2}]_{liq}}{dt}\right)_{\text{mass transfer}} = \alpha\frac{d[\mathrm{P}]_{liq}}{dt} = \frac{\alpha}{\beta}\frac{d[\mathrm{ROOH}]_{liq}}{dt} \tag{S2}$$

By integrating the differential form in Eq. S2 and equating it to the integrated rate law (Eq. 2), we get the expression:

$$\int_0^t \frac{\alpha}{\beta}\frac{d[\mathrm{ROOH}]_{liq}}{dt}dt = \int_0^t k_p\sqrt{\frac{k_i[\mathrm{ROOH}]}{k_t}}[\mathrm{RH}]^{3/2}\,dt$$

By separation of variables, this simplifies to

$$\frac{\alpha}{\beta}\int_0^{[\mathrm{ROOH}](t)}[\mathrm{ROOH}]^{-1/2}\,d[\mathrm{ROOH}]_{liq} = k_p\sqrt{\frac{k_i}{k_t}}[\mathrm{RH}]^{3/2}\int_0^t dt$$

Completing the integration yields:

$$\frac{2\alpha}{\beta}[\mathrm{ROOH}]^{1/2} = Z\cdot t \qquad \text{(S3)}$$

where

$$Z = k_{prop}\sqrt{\frac{k_{init}}{k_{term}}}[\mathrm{RH}]^{3/2} = k_{eff}[\mathrm{RH}]^{3/2}$$

The notation here is such that the experimentally obtainable rate constant (k_{eff}) is a function of rate constants of the individual, elementary reaction steps: chain initiation (k_{init}), chain propagation (k_{prop}) and chain termination (k_{term}).

Upon reshuffling of Eq. S3, we get the time-dependency of the hydroperoxide concentration as well as concentration of the sum of products, both having a quadratic form:

$$[\mathrm{ROOH}](t) = \left(\frac{\beta\cdot Z}{2\alpha}\right)^2 t^2 = \frac{\beta^2\cdot Z^2}{4\alpha^2}t^2 \qquad \text{(S4)}$$

$$[\mathrm{P}](t) = \frac{\beta\cdot Z^2}{4\alpha^2}t^2 \qquad \text{(S5)}$$

Later on, we will need the relative gas volumes as a function of time. For doing this, it becomes handy to consider the moles of oxygen reacted.

$$n(\mathrm{O_2})_{gas}(t) = n(\mathrm{O_2})_{gas}(0) - \alpha[\mathrm{P}](t)\cdot V_{liq} = \frac{p(\mathrm{O_2})}{RT}\cdot V_{gas}(0) - \alpha[\mathrm{P}](t)\cdot V_{liq}$$

This formula can be interpreted as being applied to one shrinking gas bubble (V_{gas}) with one liquid slug of constant volume (V_{liq}). After rearrangement it becomes

$$V_{gas}(t) = V_{gas}(0) - \frac{RT}{p(\mathrm{O_2})}\alpha[\mathrm{P}](t)\cdot V_{liq} = V_{gas}(0) - \frac{RT}{p(\mathrm{O_2})}\alpha[\mathrm{P}](t)\cdot\frac{V_{gas}(0)}{\gamma}$$

and the relative gas volumes can be expressed as a function of time:

$$\frac{V_{gas}(t)}{V_{gas}(0)} = 1 - \frac{\alpha}{\gamma}\frac{RT}{p(\mathrm{O_2})}\alpha[\mathrm{P}](t) \qquad \text{(eq. S6)}$$

In a next step, we want to find a correlation of the time and space, since our reactor is operating under steady-state conditions (i.e. at any given time, the concentration at a particular point in the reactor, the product concentration is constant). For this, we need to express the position (x) in the reactor as a function of time (t) and total volumetric flow rate (*TFR*), which itself is a function of the liquid volumetric flow rate (*LFR*) and gas volumetric flow rate (*LFR*). Division by the channel cross section (A) gives the respective superficial flow rates (i.e. distance per time). We treat this problem as a 1-dimensional one, i.e. analogously to the classical plug-flow assumption.

$$x = \int_0^t \frac{TFR}{A}\,dt = \int_0^t \frac{LFR + GFR}{A}\,dt == \frac{LFR}{A}\int_0^t \left(1 + \gamma\frac{V_{gas}(t)}{V_{gas}(0)}\right)dt = \frac{LFR}{A}\int_0^t \left(1 + \gamma - \alpha\frac{RT}{p(\mathrm{O_2})}Z^2\frac{\beta}{4\alpha^2}t^2\right)dt$$

$$x = \frac{LFR}{A}\left(t(1+\gamma) - \alpha\frac{RT}{p(\mathrm{O_2})}Z^2\frac{\beta}{4\alpha^2}\frac{t^3}{3}\right)$$

In particular, the time of full gas consumption will be

$$x_{end} = \frac{LFR}{A}\left(t(1+\gamma) - \alpha\frac{RT}{p(\mathrm{O_2})}Z^2\frac{\beta}{4\alpha^2}\frac{t_{end}^3}{3}\right) \qquad \text{(eq. S7)}$$

We know that once all gas is consumed, it is

$$n(\mathrm{O_2})_{gas} = 0$$

Thus, the amount of oxygen that was in the gas phase, initially, is now in the liquid phase in the form of products.

$$V_{gas}(t_0)\cdot\frac{p(\mathrm{O_2})}{RT} = V_{liq}(t_{end})\cdot\alpha[\mathrm{P}](t_{end})$$

Note: There are still some "gas" molecules dissolved in the liquid phase, but since these are actually solvated molecules and do not form any gaseous head-space. Moreover, they were also there before the reaction, when the gas-liquid equilibrium was established. So they drop out of the calculation.

By introducing the gas/liquid ratio γ, and by applying incompressibility of the liquid phase, this simplifies to

$$\gamma\cdot\frac{p(\mathrm{O_2})}{RT} = \alpha[\mathrm{P}](t_{end})$$

$$Z = \sqrt{\frac{4\alpha\gamma}{\beta}\frac{p(O_2)}{RT}\frac{1}{t_{end}^2}} = \frac{2}{t_{end}}\sqrt{\frac{\alpha\gamma}{\beta}\frac{p(O_2)}{RT}} \qquad \text{(eq. S8)}$$

Inserting eq. S8 into eq. S7 gives a very simple form, how end location (x_{end}) and end time (t_{end}) are connected:

$$x_{end} = \mathrm{LFR}_{\mathrm{sup}} \cdot t_{end}\left(1 + \frac{2}{3}\gamma\right) \qquad \text{(eq. S9)}$$

Also, by reinserting eq. S9 into eq. S8, Z can be explicitly calculated

$$Z = \sqrt{\frac{\alpha\gamma}{\beta}\frac{p(O_2)}{RT}}\, 2\mathrm{LFR}_{\mathrm{sup}}\frac{1 + {}^{2}\!/_{3}\,\gamma}{x_{end}}$$

Finally, we can get the effective rate constant by using the definition of Z:

$$k_{eff} = Z \cdot [\mathrm{RH}]^{-3/2}$$

This gives us the required formula (equation 1), where we can relate the effective rate constant (k_{eff}) with the gas bubble end position (x_{end}) in the reactor as the only observable:

$$k_{eff} = \sqrt{\frac{\alpha\gamma}{\beta}\frac{p(O_2)}{RT}}\, 2\mathrm{LFR}_{\mathrm{sup}}\frac{1 + {}^{2}\!/_{3}\,\gamma}{x_{end}}[\mathrm{RH}]^{-3/2} \qquad \textbf{(eq. 1)}$$

All other parameters are either controllable by the experimental parameters ($p(O_2)$, T, LFR_{sup}, γ) or are parameters that can be estimated by the substrate's molecular structure (α, β).

Comment: After obtaining rate constants at various temperatures, an Arrhenius evaluation gives the effective prefactor and effective activation energy for k_{eff}. The prefactor is susceptible to all parameters of equation 1. But noteworthy, the activation energy is in good approximation independent of all assumptions (!) and depends only on the robust, direct experimental quantity x_{end} (eq. 3).

$$E_A = -R\frac{\partial \ln(k_{eff})}{\partial\left({}^{1}\!/_{T}\right)} = -R\frac{\partial \ln\left({}^{1}\!/_{x_{end}}\right)}{\partial\left({}^{1}\!/_{T}\right)} \qquad \textbf{(eq. 3)}$$

Verification of equation 3 for other mechanisms

Product-assisted initiation mechanisms

It has been shown that cyclohexane autoxidation occurs with ketone-assisted hydroperoxide initiation, rather than the substrate-assisted initiation found for olefins (as detailed above). Thus, the equation 2 has to be slightly modified:

$$r_{eff} = k_{prop}\sqrt{\frac{k_{init}[\mathrm{Q{=}O}][\mathrm{ROOH}]}{k_{term}}}[\mathrm{RH}] = k_{eff}[\mathrm{ROOH}]^{1/2}[\mathrm{Q{=}O}]^{1/2}[\mathrm{RH}] \qquad \text{(eq. 2')}$$

The associated time-dependency of the sum of products is exponential, rather than quadratic (which was the result for the above mechanism, eq. S5):

$$[\mathrm{P}](t) = \frac{[\mathrm{ROOH}]_0}{\beta}\exp\left(-\frac{\alpha}{\beta}\left(\frac{\delta}{\beta}\right)^{-1/2}\right)\exp\left(k_{eff}[\mathrm{RH}]\,t\right) \qquad \text{(eq. S10)}$$

After going through a similar formula derivation as detailed above, we find the corresponding equation 1', which again describes k_{eff} as function of x_{end}:

$$k_{eff} = \frac{\mathrm{LFR_{sup}}}{[\mathrm{RH}]}\frac{1}{x_{end}}\left\{(1+\gamma)\ln\left(\frac{\gamma\beta}{\alpha[\mathrm{ROOH}]_0}\right) + \frac{(1+\gamma)\alpha}{\beta}\left(\frac{\delta}{\beta}\right)^{-1/2} + \frac{\alpha}{\beta}\frac{RT}{p(\mathrm{O_2})}[\mathrm{ROOH}]_0\exp\left(\frac{\alpha}{\beta}\left(\frac{\delta}{\beta}\right)^{-1/2}\right) - \gamma\exp\left(2\frac{\alpha}{\beta}\left(\frac{\delta}{\beta}\right)^{-1/2}\right)\right\} \qquad \text{(eq. 1')}$$

Again, the exponential temperature dependency of x_{end} is much larger than the linear temperature dependency of RT. Thus, in good approximation, the transformation done in eq. 3 is valid also for this case! This means that eq. 3 holds just as well for this mechanistic assumption.

Non-autocatalytic oxidations

In other cases, reaction rates do not depend on any of the autoxidation products. Such reactions are NOT subject to autocatalysis like the examples given above. An example for this is aldehyde autoxidation. In such a case, equation 2 has to be slightly modified to:

$$r_{eff} = k_{prop}\sqrt{\frac{k_{init}}{k_{term}}}[\mathrm{RH}] = k_{eff}[\mathrm{RH}] \qquad \text{(eq. 2")}$$

The associated time-dependency of the sum of products is linear, rather than quadratic or exponential (which were the results for the above mechanisms, eqs. S5 and S10):

$$[\mathrm{P}](t) = \frac{1}{\alpha}k_{eff}[\mathrm{RH}]\,t \qquad \text{(eq. S11)}$$

After going through a similar formula derivation as detailed above, we find the corresponding equation 1", which again describes k_{eff} as function of x_{end}:

$$k_{eff} = \frac{\mathrm{LFR_{sup}}}{[\mathrm{RH}]} \frac{1}{x_{end}} \left\{ \frac{p(\mathrm{O_2})}{RT} \gamma \left(1 + \frac{\gamma}{2} \right) \right\} \qquad \text{(eq. 1")}$$

Again, the exponential temperature dependency of x_{end} is much larger than the linear temperature dependency of RT. Thus, in good approximation, the transformation done in eq. 3 is valid also for this case! This means that eq. 3 holds just as well for this mechanistic assumption.

Internal coordinate system of the microreactor

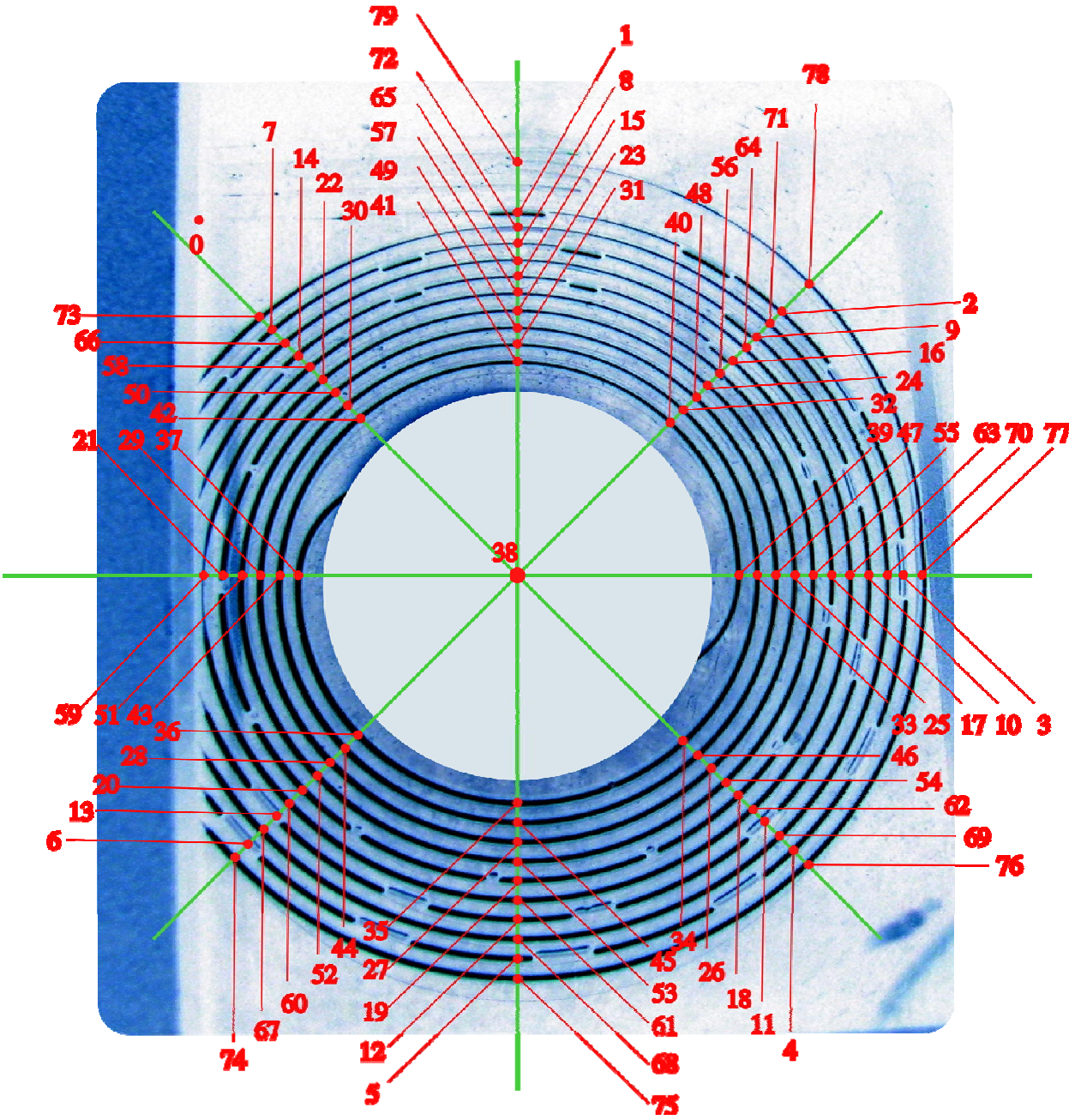

Figure S1. Internal coordinate system of the spiral microreactor (inverted colors for clarity). Gas bubbles are darkish on the upper half and bright on the lower half.

For visual read-out of the experimental data, i.e. the reaction end-point x_{end}, we defined and calibrated an internal coordinate system (Figure S1 and Table S1). 80 points were defined along the reactor's principal axes and bisecting lines. The numbering runs from 0 to 79. Since the reactor is 0.85 m long, the average mesh size is 10.8 mm. However, with interpolation between

the distinguished points, the effective mesh size was 5.4 mm. For instance, in the case of Figure S1, x_{end} is between points 21 and 22, giving an interpolated value of 21.5.

Table S1. Internal coordinate system of the spiral microreactor. Distance conversion table from [point number] in the first and third column to [mm] in the second and fourth columns. Includes interpolated values.

0	0	40.5	433
0.5	10	41	436
1	19	41.5	441
1.5	25	42	445
2	32	42.5	450
2.5	38	43	454
3	44	43.5	459
3.5	50	44	463
4	57	44.5	468
4.5	63	45	472
5	69	45.5	476
5.5	75	46	480
6	80	46.5	484
6.5	91	47	488
7	102	47.5	492
7.5	108	48	496
8	113	48.5	500
8.5	119	49	504
9	125	49.5	508
9.5	131	50	513
10	137	50.5	517
10.5	143	51	521
11	150	51.5	525
11.5	156	52	530
12	162	52.5	534
12.5	173	53	538
13	183	53.5	543
13.5	194	54	547
14	204	54.5	552
14.5	209	55	556
15	214	55.5	560
15.5	219	56	564
16	224	56.5	568
16.5	231	57	572
17	237	57.5	577
17.5	244	58	582
18	250	58.5	586
18.5	252	59	591
19	254	59.5	595
19.5	258	60	599
20	261	60.5	603
20.5	263	61	607
21	265	61.5	612
21.5	270	62	618
22	276	62.5	623
22.5	281	63	628
23	286	63.5	633
23.5	291	64	638
24	295	64.5	642
24.5	300	65	647
25	304	65.5	653
25.5	308	66	659
26	312	66.5	671
26.5	316	67	682
27	320	67.5	688
27.5	324	68	694
28	328	68.5	700
28.5	332	69	707
29	336	69.5	713
29.5	340	70	719
30	345	70.5	725
30.5	349	71	731
31	353	71.5	736
31.5	357	72	742
32	360	72.5	750
32.5	364	73	757
33	367	73.5	772
33.5	371	74	787
34	374	74.5	795
34.5	378	75	802
35	381	75.5	808
35.5	385	76	814
36	389	76.5	820
36.5	392	77	826
37	396	77.5	832
37.5	399	78	838
38	401	78.5	844
38.5	412	79	850

39	422
39.5	426
40	429